https://doi.org/10.20965/jrm.2021.p0665

Paper:

Gap Traversing Motion via a Hexapod Tracked Mobile Robot Based on Gap Width Detection

Taiga Sasaki and Toyomi Fujita

Department of Electrical and Electronic Engineering, Faculty of Engineering, Tohoku Institute of Technology
35-1 Yagiyama Kasumi-cho, Taihaku-ku, Sendai 982-8577, Japan
E-mail: {d181901@st., t-fujita@}tohtech.ac.jp
[Received July 20, 2020; accepted March 26, 2021]

The authors developed a hexapod tracked mobile robot: a tracked mobile robot which is equipped with six legs attached to the robot's body. In a transportation task, this robot can traverse a wide gap by supporting track driving with four front and rear legs while holding the target object with its two middle legs. To realize autonomous actions with this robot, we developed a two-dimensional distance measurement system using an infrared sensor. This system is very simple, with the sensor attached to a servomotor, such that it does not require high computing power for measurement. In addition, the system can be equipped at a lower cost than laser range finders and depth cameras. This paper describes the selection of the gap traversing mode according to gap width detected by the system. In this study, we conducted a gap width detection experiment and an autonomous gap traversing experiment using the hexapod tracked mobile robot with the proposed system. The obtained results confirm the effectiveness of the proposed system and autonomous traversing, which corresponds with the gap width detection.

Keywords: hexapod tracked mobile robot, hybrid motion by tracks and legs, two-dimensional distance measurement system, autonomous gap traversing

1. Introduction

In recent years, several studies have considered robot technologies to enable robots perform certain handling tasks on behalf of humans, such as transportation tasks in disasters and dangerous sites [1–4]. Accordingly, to productively work on uneven terrains, robots are required to exhibit high working and moving abilities. Therefore, the authors have developed a hexapod tracked mobile robot equipped with six legs and four degrees-of-freedom mechanisms, which can be adopted as working arms in track movements [5, 6], as illustrated in **Fig. 1**. It is feasible to support track driving using four front and rear legs to traverse a wide gap while holding and transporting an object with two middle legs. In a previous study, we experimented and investigated the leg-track hybrid motion for gap traversing in an object transportation task [7].

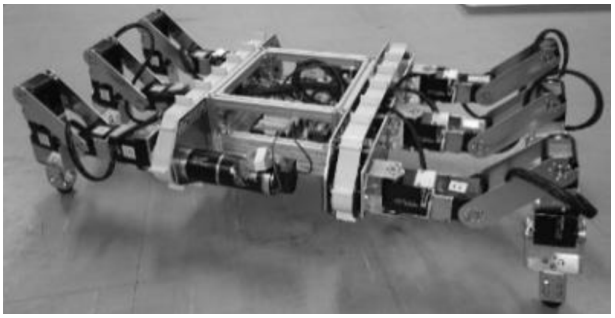

Fig. 1. Hexapod tracked mobile robot.

The objective of this study is to realize autonomous gap traversal for the hexapod tracked mobile robot via gap width detection. Accordingly, we consider selecting the modes of gap traversing motion based on the detected gap width. To detect the gap width, we developed a two-dimensional distance measurement system using a one-dimensional distance sensor and a motor. Based on this measurement system, the width of the gap can be detected by measuring the distance to the road surface in front. According to the detected gap width, the robot can select an appropriate motion mode for gap traversal. In this paper, we describe the proposed method and experimental results for the autonomous gap traversal of a hexapod tracked mobile robot.

2. Related Works

In this study, we consider the autonomous gap-traversing motion. The robot's mechanism is essential in appraising the performance of gap traversal performance. Generally, a tracked robot can traverse a gap with a width of approximately 45% of the track length, which touches the ground at the maximum [8]. Although the robot length is also an important factor for performance, in this study, we consider its relationship with the length of the track based on this knowledge.

Most of the studies that have considered gap traversing primarily adopted tracked mobile robots for their research. For example, "RT05-COBRA" [9], developed by

Kinugasa et al., is a tracked robot with a flexible monotread mobile track (FMT). This robot is covered with FMT all over its body and can perform 3-D motion by solely using a flexible track. The length of the track that touches the ground is the same as the total length of the robot, 1.2 m. It was confirmed that the robot traversed a gap width of approximately 550 mm.

The "KOHGA" [10], developed by Kamekawa et al., is a snake-type robot that connects four small tracked robots. Based on running experiments, gap traversing was achieved for a maximum gap width of 350 mm and a total length of 740 mm of the track touching the ground.

In addition, "TITAN X" [11], developed by Hodoshima et al., is a robot with a leg mechanism that is driven by a track, and can perform cooperate motion with the legs and the tracks. The total length of the robot's running surface was 890 mm. This robot realized 400 mm-wide track driving based on an experiment.

In addition, "Quince" [12], developed by Rohmer et al., has a structure in which sub-flippers are attached to the four corners of the main tracks. By deploying the sub-flipper, it is possible to increase the overall length of the robot and leg contact position, as well as the gap width to traverse. Because the total length of the main and sub-tracks is 1110 mm, a gap traversing of approximately 500 mm is feasible.

"Scott" [13], developed by Suzuki et al., has a similar configuration to "Quince," which consists of main tracks and passive sub-tracks. Because the robot has a total length of 720 mm, it is possible to traverse a gap width of approximately 324 mm.

"R-5S" [14], developed by Murakami et al., has a similar configuration to "Quince." Therefore, similar to the already mentioned robots, the gap traversing motion is possible by the sub and main tracks.

"UMRS" [15], which was developed by Kobayashi et al., is a tracked robot with a total track running surface length of 480 mm, including flippers that touch the ground. This robot was able to traverse a gap width of approximately 240 mm.

In general, as can be observed from these studies, it is difficult for a conventional tracked robot to traverse a gap with a width more than half the length of the track touching the ground. However, the hexapod tracked mobile robot developed by the authors can traverse a gap wider than it by using its legs to assist track driving, as illustrated in **Fig. 2**. In our previous research, the traversal of a 260-mm gap width, 130% of a 200-mm track length, was realized [7].

For autonomous navigation, sensing and mapping the surrounding environment is essential. Most of the environment mapping methods for autonomous mobile robots adopt imaging cameras, laser range finders (LRFs), or depth image sensors.

In the case of imaging cameras that adopt stereo vision with a color camera, a 3-D map is generated from the feature points of the images of single or multiple cameras, and then navigation is executed [16, 17]. However, the calculation cost of extracting the feature points of the image set is high, and the error tends to be more significant than that of other methods.

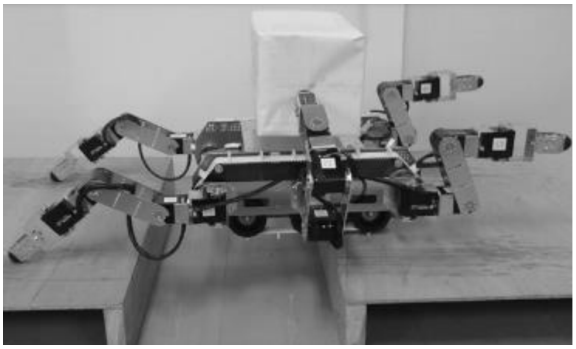

Fig. 2. Gap traversing in transportation of a box-type object.

Regarding the LRF, a 2-D map from the distance data around the sensor axis can be generated by the LRF [18–21]. Its accuracy is better than that of stereo vision, and it can reduce calculation costs. In addition, it is possible to map the area around a robot over a wide range. However, because its minimum measurable distance is approximately 0.5 m, the LRF is mainly utilized for long-distance measurements of 3–5 m; therefore, it is not suitable for measuring environments close to the robot.

In the case of adopting depth image sensors, 3-D map generation and navigation can be performed based on point cloud distance data [22–25], which has been introduced in recent environment mapping. The point cloud can be output directly from the data, such that the distance data from any point can be easily acquired. However, this approach requires a CPU with a large computing power because calculation costs increase when processing the point cloud data.

For autonomous gap traversing, which is the focus of this study, the robot can sufficiently measure short distances to the ground in a certain range to detect a gap width in front of the robot. Therefore, we developed and installed a distance measurement system in which an infrared distance sensor capable of measuring short distances is attached to a servomotor. This system can generate a 2-D map; hence it is similar to the LRF structure. Moreover, both development and calculation costs can be more significantly reduced with this approach than with other environmental recognition methods already mentioned.

In this study, the gap width was determined using the installed distance measurement system. The purpose is to enable the robot to realize autonomous wide-gap traversing.

3. Autonomous Gap Traversing

3.1. Gap Traversing Motion

Figure 3 presents an overview of the gap traversing by the hexapod tracked mobile robot. This figure illustrates the side view of the robot. For simplification, we assumed

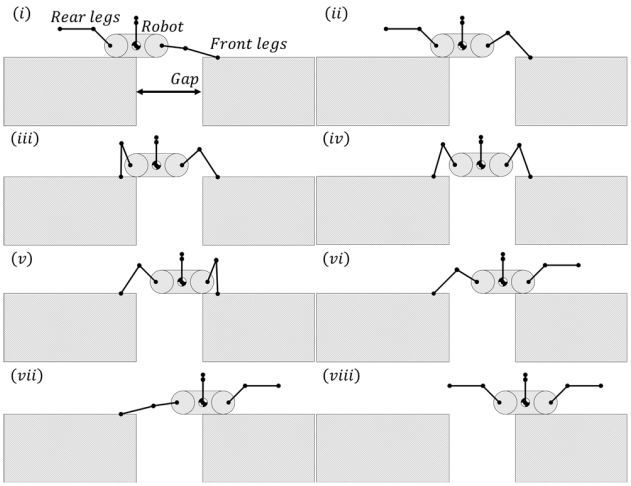

Fig. 3. Gap traversing motion.

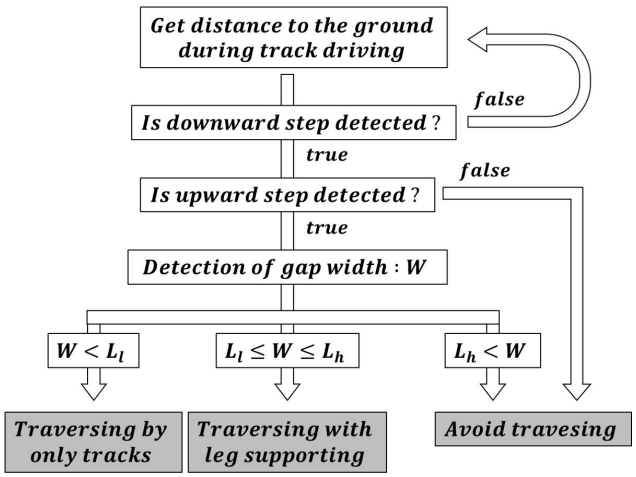

Fig. 4. Gap traversing algorithm.

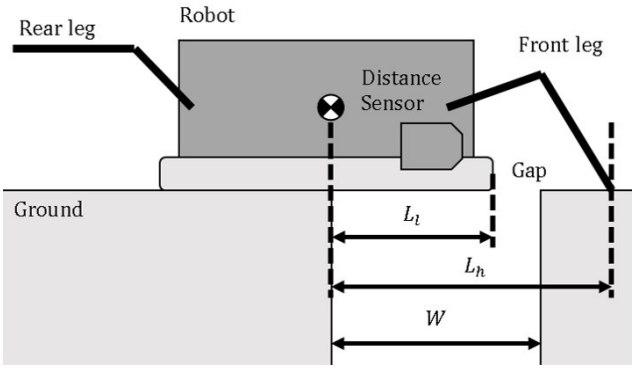

Fig. 5. Two-dimensional model of gap traversing.

that the heights of the ground between the gaps were the same, the road surface was almost flat without significant unevenness, the gap width was constant, and the robot traveled orthogonally to the gap.

When the robot moves by tracks and the front part of the body reaches the gap, the robot touches the tips of its front legs at a small distance before the edge on the far side, before its center of gravity approaches a position just above the gap's edge (i). At this point, the robot can continue moving forward using its tracks by supporting itself with the tips of the front legs (ii). Then, the robot touches the tips of the rear legs slightly behind the edge on the near side before its body is completely suspended above the gap (iii). Then, the robot crosses the gap by supporting the body using the front and rear legs (iv). When the front end position of the body touches the ground on the far side, the robot releases the tips of its front legs from the ground (v). Then, the robot continues moving forward, propelled by its tracks with its rear leg tips supporting it (vi). When the center of gravity of the robot's body reaches the ground on the far side, the robot can release the tips of its rear legs (vii), and then return to normal locomotion using only its tracks (viii).

3.2. Algorithm

Figure 4 presents an overview of the control algorithm for the gap traversing achieved by the gap width detection of the hexapod tracked mobile robot equipped with a distance measurement system, which will be described in Section 4.1.

By assuming that the robot travels on a flat road surface, the distance between the robot and the road surface ahead is acquired by the measurement system. At this point, if the distance increases significantly, it can be estimated that a step exits in the downward direction.

Then, the presence or absence of an upward step is determined from the distance information in the further front area. If the step is not detected, it is assumed that the gap is too long to traverse, such as a valley or a cliff. In this case, the robot stops moving to avoid traversing. Conversely, if step is detected, it is determined that there is a gap in the front. In this case, the gap width is detected via the method described in Section 4.2.

When the gap width is detected, the robot determines the appropriate action corresponding to the width. Let W, L_l, and L_h represent the detected gap width, maximum gap width by which the robot can solely traverse via track running, and the maximum gap width by which the robot can traverse the gap with leg support, respectively. If $W < L_l$, the robot can continue driving through the tracks. However, if $L_h < W$, the track exceeds the width that the robot can traverse. If $L_l \leq W \leq L_h$, gap traversal is realized with the assistance of leg support, as illustrated by a 2-D model presented in **Fig. 5**.

In the traversing mode with leg support, the robot initially drives until the center of gravity reaches the edge of the rear gap. Then, the front legs touch the front road surface. The robot moves forward by driving track with the support of the front legs. When the rear end of the track reaches the edge of the rear gap, the rear legs touch the road surface on the rear side. Subsequently, the robot moves with four legs. When the front end of the track arrives at the edge of the front gap, the robot releases its front legs and moves forward with its rear legs. Finally,

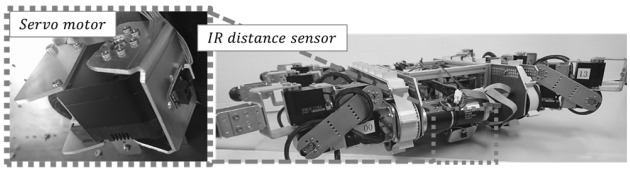

Fig. 6. Two-dimensional distance measurement system.

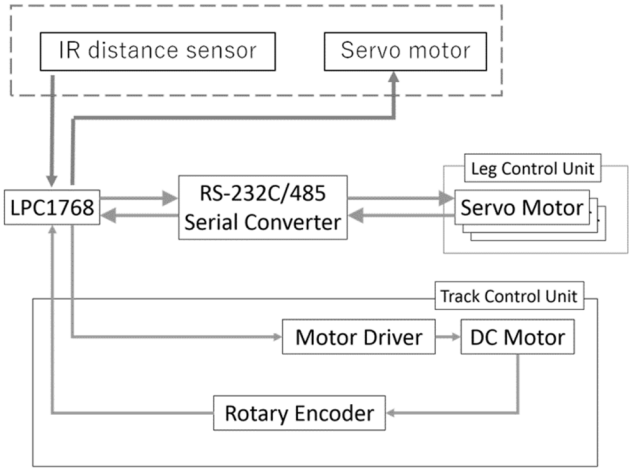

Fig. 7. Robot control system.

when the robot's center of gravity arrives at the edge of the gap's front, the robot releases its rear legs and completes the gap traversing.

4. Gap Width Detection

4.1. Gap Detecting System

Figure 6 presents the manufactured distance measurement system. This system was installed on a hexapod tracked mobile robot developed by the authors. The measurement system can obtain 2-D distance information by rotating a 1-D infrared distance sensor using a motor. The sensor was mounted 23 mm from the motor rotation axis while the measurement system was mounted 35 mm from the bottom of the body and 50 mm from the front of the robot. Sharp GP2Y0E03 and Kondo Kagaku B3M-SC-1170-A were adopted as an infrared sensor and a motor, respectively.

Figure 7 illustrates the configuration of the control system installed in the robot. The rotation angle of the sensor was controlled by the mbed microcomputer LPC1768, and the distance at each angle was determined. This mechanism enables the measurement system to obtain 2-D distance information beforehand. The configuration of this system is very simple and does not require high computing power for its measurement. In addition, the measurement system can be implemented at a lower cost than a laser range finder, depth camera, etc.

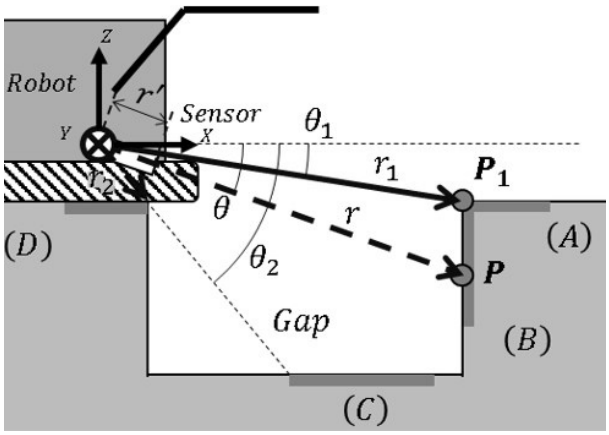

Fig. 8. Gap width detection model.

4.2. Method

As described in Section 3, the presence or absence of a gap can be determined by detecting the step in the vertical direction, and the corner on each road surface becomes the gap edge. The gap width detection method is described as follows.

Figure 8 illustrates the gap width detection model. As described in Section 3.1, we assumed that the heights of the ground between the gaps were the same, the road surface was almost flat without any large unevenness, the width of the gap was constant, and the robot traveled orthogonally to the gap. Furthermore, we assumed that the wall surface of the gap is vertical to the ground, and the angle between the wall and road surfaces on the edge is 90°. Consider a sensor coordinate system with the motor as its origin, the Y-axis corresponds to the rotation axis of the motor, and the X-axis faces the forward direction of the robot. When the sensing direction is parallel to the X-axis, it is assumed to be a 0° angle rotation of the sensor. The sensor rotates from 0° in the positive direction around the Y-axis. The dashed arrow in **Fig. 8** represents the distance measured at the sensor angle θ. When the measured distance at this point is r, the measured position $\boldsymbol{P}$ is given by:

$$\boldsymbol{P} = \left[(r+r')\cos\theta \quad 0 \quad -(r+r')\sin\theta \right]^{\mathrm{T}}, \quad . \quad (1)$$

where r' is the distance from the origin of the sensor coordinate system to the distance measurement sensor, and T indicates the transpose of the matrix.

At the beginning, if a downward step is detected, the sensor initially rotates to zero once, and then starts rotating to positive angles. Subsequently, the upper surface of the step on the far side of the robot ((A) in **Fig. 8**) will be detected if a gap exists. Then, the measured distance r decreases as the sensor angle increases, and its derivative $(dr/d\theta)$ becomes negative.

When the sensor angle is further increased, the vertical wall surface in the gap ((B) in **Fig. 8**) is detected. At this point, r increases with θ, and $(dr/d\theta)$ becomes positive. Therefore, by adopting the sensor angle θ_1 and the measured distance r_1 when $(dr/d\theta)$ changes from negative to

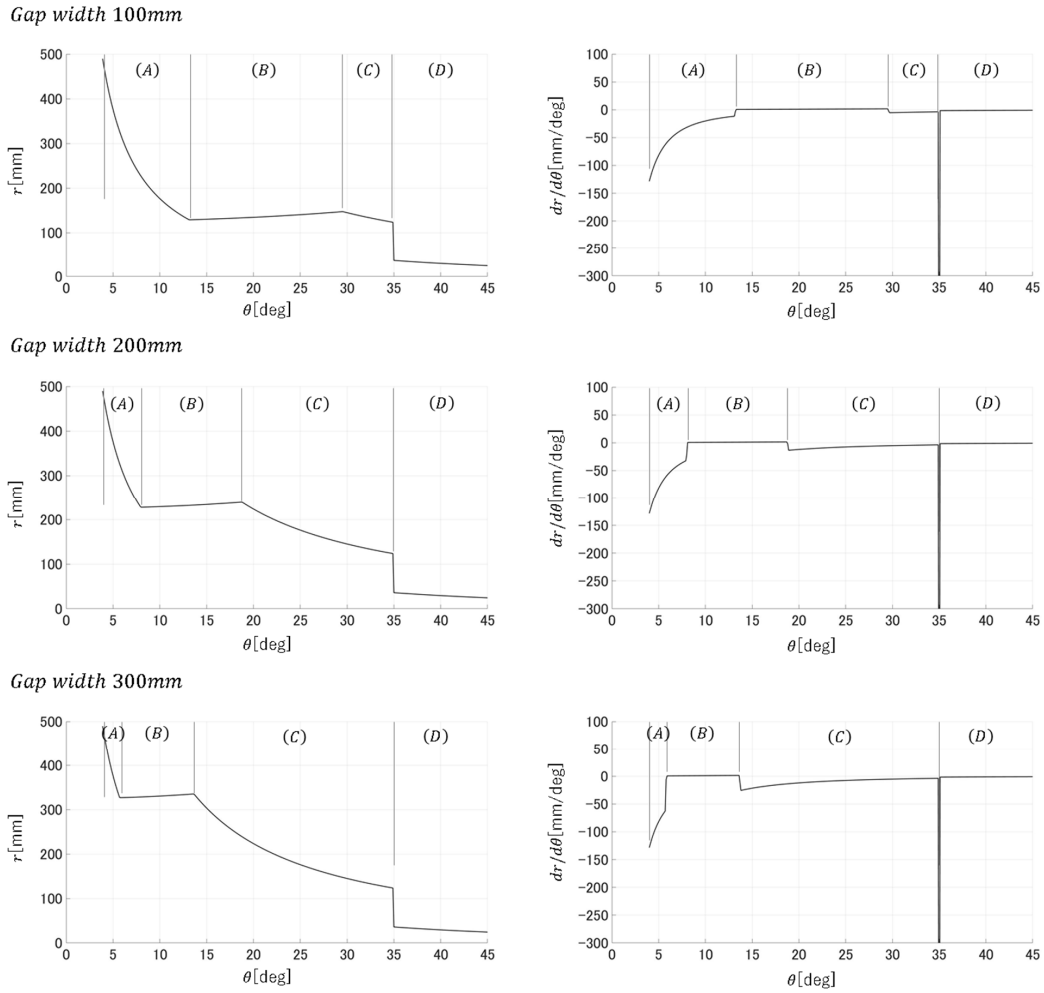

Fig. 9. Simulation results: detected distance to sensor angle (left) and derivative of detected distance to sensor angle $(dr/d\theta)$ (right).

positive, the position $\boldsymbol{P}_1$ of the gap edge on the far side can be obtained from Eq. (1). As the sensor angle is further increased, the bottom of the gap ((C) in **Fig. 8**) will be detected.

Then, when the road surface of the robot side ((D) in **Fig. 8**) is detected, r abruptly decreases. Therefore, the position $\boldsymbol{P}_2$ of the gap edge on the near side can be obtained from the measured distance r_2 corresponding to the sensor angle θ_2 when $(dr/d\theta)$ is minimum.

If the gap is deep, the measured distances become invalid for (C) in **Fig. 8** because the distance exceeds the sensing range. In this case, we can obtain $\boldsymbol{P}_2$ in the same way by replacing these invalid values with the maximum detectable values of the sensor.

From the obtained $\boldsymbol{P}_1$ and $\boldsymbol{P}_2$, the gap width W is given by:

$$W = [1 \quad 0 \quad 0](\boldsymbol{P}_1 - \boldsymbol{P}_2) \quad . \ . \ . \ . \ . \ . \ . \ . \ . \quad (2)$$

When applying this method for gap width detection, a calculation error occurs owing to the resolution of the sensor rotation angle. Let $\boldsymbol{P}_n = [x_n \quad y_n \quad z_n]^{\mathrm{T}}$, θ_n, and $\Delta\theta$ represent the position of the n-th gap edge, detected angle of $\boldsymbol{P}_n$, and resolution of the sensor rotation angle, respectively. Then, the maximum error value of the gap width Δx_n is defined by:

$$\Delta x_n = -z_n \left(\frac{1}{\tan(\theta_n - \Delta\theta)} - \frac{1}{\tan\theta_n} \right). \quad . \ . \ . \quad (3)$$

4.3. Simulation

We conducted a simulation for gap width detection based on the method described above. In this simulation, the width of the gap W was set to 100, 200, and 300 mm, and the depth of the gap was set to 50 mm. The robot was positioned, such that the front end of the robot coincided with the gap edge on the near side. Therefore, $\boldsymbol{P}_1$ and $\boldsymbol{P}_2$ are $\boldsymbol{P}_1 = [W+50 \quad 0 \quad -35]^{\mathrm{T}}$ and $\boldsymbol{P}_2 = [50 \quad 0 \quad -35]^{\mathrm{T}}$ mm. We calculated the measured distance from 0° to 45° sensor angles because the angle for $\boldsymbol{P}_2$ was 34.99° while the resolution of the rotation angle was set to 0.1°.

Figure 9 presents the simulation results. The left panel presents the measured distance to the sensor angle, and the right panel depicts the derivative $(dr/d\theta)$, which represents the magnitude of change in the detected distance relative to the angle. The detected parts (A), (B), (C), and (D) are also depicted. The computed edge positions and gap widths are presented in **Table 1**.

Table 1. Simulation result of gap width detection.

Gap width [mm]	100	200	300
$\boldsymbol{P}_1$ [mm]	$\begin{bmatrix} 149.9 \\ 0 \\ -35.2 \end{bmatrix}$	$\begin{bmatrix} 250 \\ 0 \\ -35.1 \end{bmatrix}$	$\begin{bmatrix} 150 \\ 0 \\ -35.6 \end{bmatrix}$
Error of $\boldsymbol{P}_1$ [%]	$\begin{bmatrix} 0.06 \\ 0 \\ -0.4 \end{bmatrix}$	$\begin{bmatrix} 0 \\ 0 \\ -0.2 \end{bmatrix}$	$\begin{bmatrix} 0.02 \\ 0 \\ -1.2 \end{bmatrix}$
$\boldsymbol{P}_2$ [mm]	$\begin{bmatrix} 49.9 \\ 0 \\ -35.0 \end{bmatrix}$		
Error of $\boldsymbol{P}_2$ [%]	$\begin{bmatrix} 0.2 \\ 0 \\ -0.4 \end{bmatrix}$		
Computed gap width [mm]	100	200.1	300

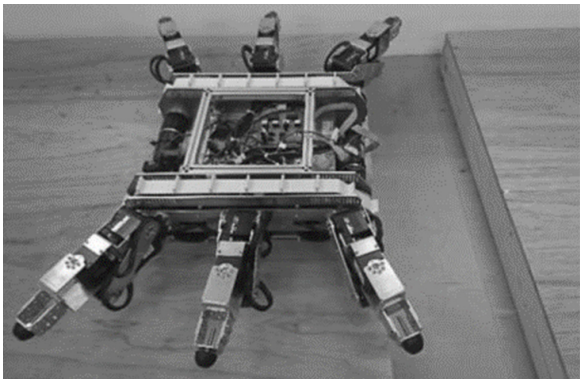

Fig. 10. Experimental setup.

In this simulation, the resolution of the rotation angle was set to 0.1°. Because the exact angles of $\boldsymbol{P}_1$ are 13.13°, 7.97°, and 5.71° for gap widths of 100, 200, and 300 mm, respectively, the maximum errors of $\boldsymbol{P}_1$ calculated by Eq. (3) are 0.8%, 1.3%, and 1.8% for gap widths of 100, 200, and 300 mm, respectively. Similarly, the error of $\boldsymbol{P}_2$ is 0.36% because its exact angle is 34.99°. It should be noted that this is the maximum error when the gap edge does not arrive at the exact angle.

The obtained results indicate that this detection method is sensitive to the sensor angle, especially for the far edge, and there is a possibility that errors may increase owing to slight deviations and robot tilts.

5. Experiments

5.1. Gap Width Detection

Several experiments were performed for gap width detection using the developed distance measurement system. **Fig. 10** illustrates the experimental environment. Two steps with heights of 50 mm were arranged at intervals of 100, 200, or 300 mm to create each gap width. In this experiment, the robot was positioned such that the front end of the robot becomes the gap edge, similar to the simulation. Ten measurements were performed for each gap width.

Figure 11 presents the measurement results of the sensor angle when the gap width is 100, 200, and 300 mm and depth is 50 mm. In this experiment, the rotation angle's resolution was set to 0.5°. The left and right panels of **Fig. 11** depict the measured distances to the sensor angles, and its derivative $(dr/d\theta)$, respectively. The r' value in Eq. (1) is 23 mm, as stated in Section 4.1. The detected parts from (A) to (D) of the gap are also indicated as an example; these borders were calculated using the average of 10 measurement data.

Figure 12 presents comparisons of the measured distances to the simulation. The dotted and black lines in **Fig. 12** represent the average value of the experimental results and the simulation results, respectively.

Table 2 presents the edge position and gap width detection results for each gap width. Here, the variance and average of ten measurements are presented. The gap width was the average value of ten measurements in which it was calculated by each set of two edge positions.

Regarding the 100-mm result, **Fig. 11** indicated that the averages of the sensor angles and measured distances were respectively 13.5° and 129.3 mm for $\boldsymbol{P}_1$, and 35.0° and 32.7 mm for $\boldsymbol{P}_2$. The measured distance results did not exhibit a significant difference, as presented in **Fig. 12**.

Therefore, the error ratio for the average of the detected X position of $\boldsymbol{P}_1$ was 1.2%, as presented in **Table 2**, whereas that of the detected gap width was 2.5%.

For the 200-mm result, **Fig. 11** indicated that the average of sensor angles and measured distances were respectively 9.5° and 241.0 mm for $\boldsymbol{P}_1$, and 35.0° and 32.1 mm for $\boldsymbol{P}_2$. As illustrated **Fig. 12**, the corner of the boundary part of (A) and (B) was rounded at an angle of 8.0°. We assumed that the $\boldsymbol{P}_1$ error was larger than 100 mm because of this effect. In fact, **Table 2** shows that the error ratio for the average of the detected X position of $\boldsymbol{P}_1$ was 4.2%, which is larger than that of the 100 mm gap width. Consequently, the error in the detected gap width was 7.4%.

Regarding the 300-mm result, **Fig. 11** shows that the average sensor angle and measured distance were respectively 9.5° and 343.6 mm for $\boldsymbol{P}_1$, and 35.0° and 33.1 mm for $\boldsymbol{P}_2$. The results presented in **Fig. 12** indicate that the error between the simulation and the experiment increased at a sensor angle of approximately 10°. Therefore, the error ratio for the average of the detected X position of $\boldsymbol{P}_1$ was 3.2%, as presented in **Table 2**.

However, it was smaller than that of the 200-mm gap width. Consequently, the error in the detected gap width was smaller than that of the 200-mm result (5.6%). Regarding the detection of $\boldsymbol{P}_1$, the results in **Table 2** indicate that the edge positions were detected stably because the variance values were negligible for every gap width. In addition, the detected position of $\boldsymbol{P}_1$ exhibited an error of

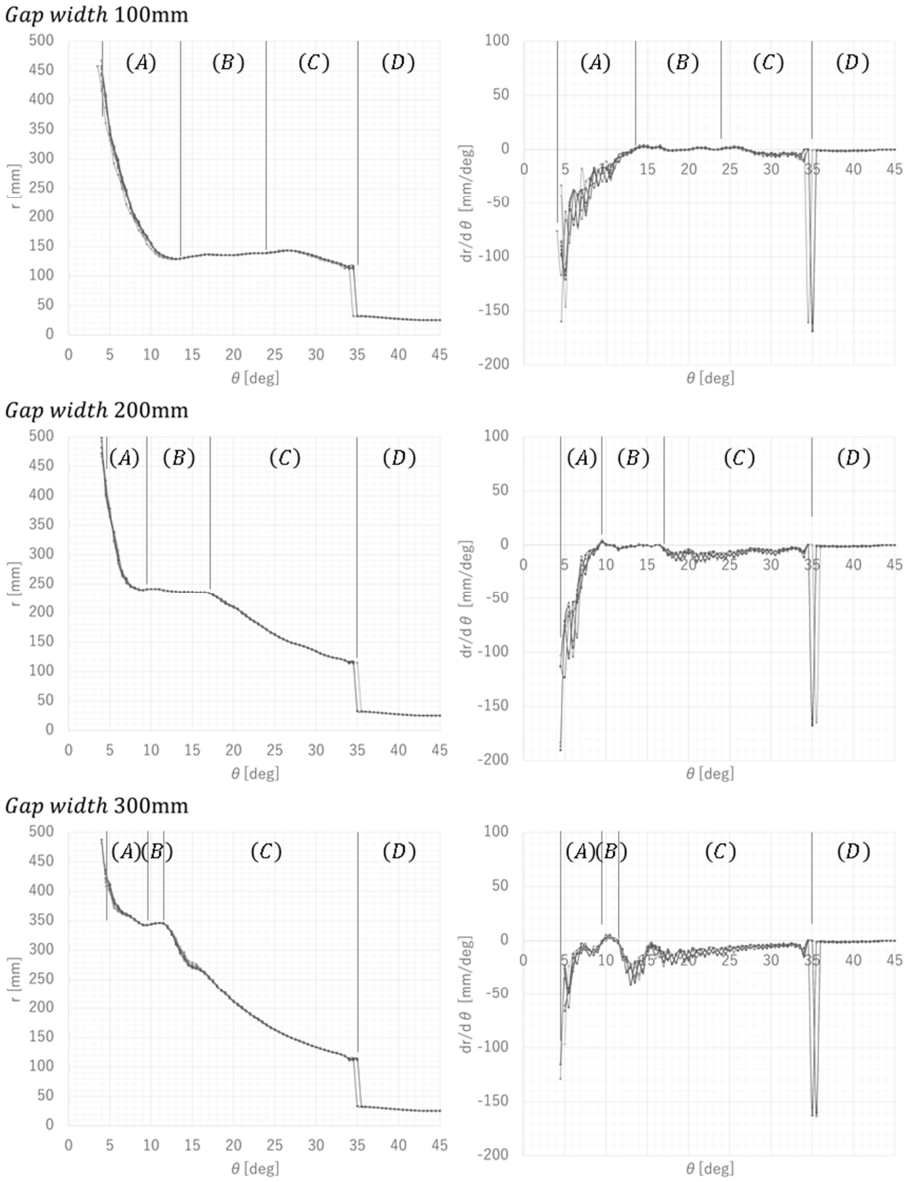

Fig. 11. Experimental results for 100, 200, and 300 mm gap widths: measured distance to sensor angle (left), and derivative of detected distance to sensor angle (right).

4% or less. As already mentioned, the maximum error triggered by the resolution of the sensor rotation angle $\Delta\theta$ is defined by Eq. (3). When $\Delta\theta$ is 0.5°, the error ratio values of $\boldsymbol{P}_1$ are 4.1% and 6.8% at 200 mm, and 9.7% at 100, 200, and 300 mm, respectively. Therefore, it can be observed that detection was achieved with sufficient accuracy.

However, the $\boldsymbol{P}_2$ error was significant (8.8%), as presented in **Table 2**. Because the maximum error triggered by the resolution of the sensor angle is 0.02% for $\boldsymbol{P}_2$, we assumed that the errors of the edge position were generated owing to sensory characteristics rather than the resolution of the sensor rotation angle. The light-receiving range in which the distance sensor can accurately measure the distances is 6° (±3°). If different factors, such as the ambient lights from the edge of the gap, are measured in this light-receiving range, the measurement system detects an incorrect distance. In the simulation, we did not consider this type of error in the distance measurement sensor. However, according to the results of the experiment, we inferred that the error appeared around the edge because the measurement system measured the wall of the gap and the surface of the road. Therefore, the error for $\boldsymbol{P}_2$ increased more significantly than that of the simulation.

To perform more accurate measurements via this method, measurements should be performed at positions sufficiently close to the gap edge to cover the gap edges in most sensing ranges. Alternatively, a robot should adopt a sensor with high directivity.

We assumed that the gap-width error in **Table 2** is permissible for gap traversing by the methods presented in **Figs. 3** and **4**, which is realized by providing a margin to the gap width when selecting the traversing mode. Therefore, these results validate the effectivity of detecting gap

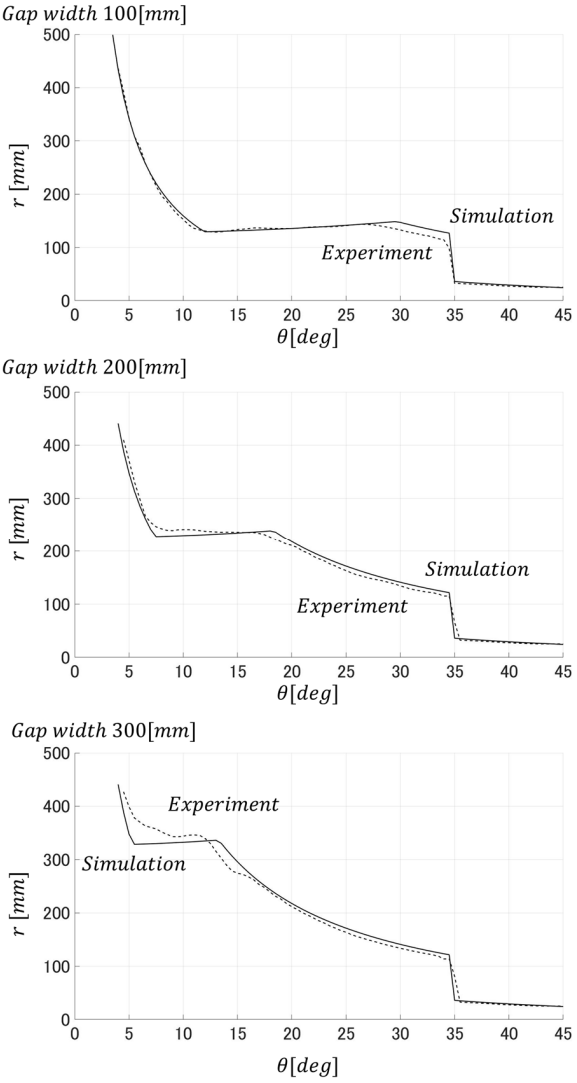

Fig. 12. Comparison of measured distance with the simulation for 100, 200, and 300 mm gap widths.

width via the proposed method with the developed measurement system.

5.2. Gap Traversing

We conducted several gap traversal experiments using the developed hexapod tracked mobile robot based on the proposed gap width detection system. The experimental environment was the same as that described in the previous section, and gap traversing was performed for gap widths of 100, 200, and 300 mm.

First, the robot was set at a distance of 250 mm or more from the gap and moved in the direction of the gap by track driving at a speed of approximately 50 mm/s. During this time, the distance to the road surface obliquely downward and forward of the robot was measured by the distance measurement system, and the magnitude of the change in the distance was obtained. When the distance-measuring system detected the amount of change equal to or greater than the threshold value, the robot stopped driving, and the gap width was obtained by the method

Table 2. Result of detection of gap width and edge positions.

Gap width [mm]	**100**	**200**	**300**
Average $\boldsymbol{P}_1$ [mm]	$\begin{bmatrix} 148.2 \\ 0 \\ -35.4 \end{bmatrix}$	$\begin{bmatrix} 260.5 \\ 0 \\ -43.4 \end{bmatrix}$	$\begin{bmatrix} 361.3 \\ 0 \\ -62.2 \end{bmatrix}$
Variance $\boldsymbol{P}_1$ [mm^2]	$\begin{bmatrix} 0.06 \\ 0 \\ 0.21 \end{bmatrix}$	$\begin{bmatrix} 0.22 \\ 0 \\ 0.58 \end{bmatrix}$	$\begin{bmatrix} 0.95 \\ 0 \\ 5.39 \end{bmatrix}$
Error of $\boldsymbol{P}_1$ [%]	$\begin{bmatrix} -1.2 \\ 0 \\ 1.2 \end{bmatrix}$	$\begin{bmatrix} 4.2 \\ 0 \\ 24 \end{bmatrix}$	$\begin{bmatrix} 3.2 \\ 0 \\ 77 \end{bmatrix}$
Average $\boldsymbol{P}_2$ [mm]	$\begin{bmatrix} 45.6 \\ 0 \\ -31.9 \end{bmatrix}$		
Variance $\boldsymbol{P}_2$ [mm^2]	$\begin{bmatrix} 0.01 \\ 0 \\ 0.01 \end{bmatrix}$		
Error of $\boldsymbol{P}_2$ [%]	$\begin{bmatrix} -8.8 \\ 0 \\ -8.9 \end{bmatrix}$		
Gap width [mm]	102.5	214.7	315.6
Variance gap width [mm^2]	0.10	0.19	1.63
Error of gap width [%]	2.5	7.4	5.2

described in Section 4.2. According to the detected gap width, the appropriate motion was selected using the method described in Section 3. In this experiment, the sensor angle in the initial track driving was set to 30°, and the threshold for the distance change was set to 100 mm.

In this experiment, the threshold L_l for the selection of the gap traversing motion was set to 100 mm by mechanical constraints. Regarding L_h, we considered the margin for safe traversing. Based on the maximum error rate in the previous experiment presented in **Table 2**, we set L_h, which was 270.1 mm in the theory by the mechanical constraint, at a margin value of 7.5%. Therefore, L_h was set to 249.8 mm.

Figures 13 and **14** illustrate the traversing motions of the robot for gap widths of 100 and 200 mm, respectively. The numbers in each figure indicate the order of the motion.

As illustrated in **Fig. 13**, the robot commenced driving in ①. Next, the robot stopped driving when the gap width was detected by the measurement system ②. The detected width was $W = 97.4$ mm for a gap width of 100 mm. Hence, $W < L_l$, which means that the robot determined that traversing was possible solely by track driving according to the algorithm described in **Fig. 4**. Then, the robot solely traversed the gap with track driving ③ and completed the motion ④.

In **Fig. 14**, the robot starts driving ① and detects a gap. Its width was $W = 213.2$ mm for the gap width of

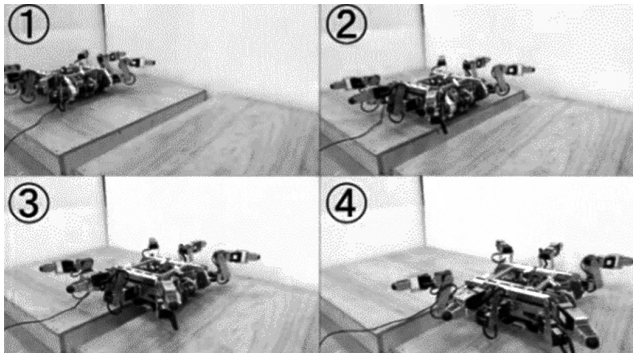

Fig. 13. Gap traversal experiment for 100 mm gap width. The robot achieved gap traversal by solely adopting track driving.

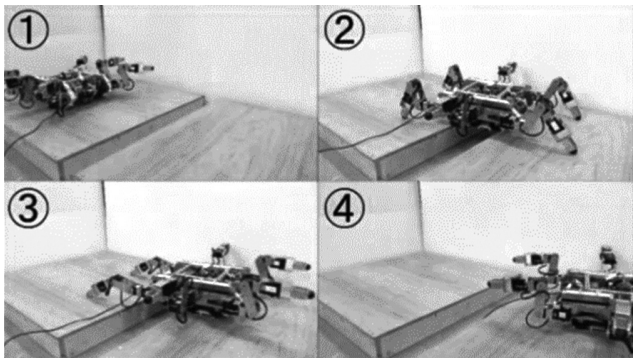

Fig. 14. Gap traversal experiment for 200 mm gap width. The robot achieved traversal with leg supports.

200 mm. Hence, $L_l \leq W \leq L_h$, such that the robot determined the gap traversing with the supporting legs, as illustrated in **Fig. 4**. The front legs were then moved to support track driving ②. Subsequently, the robot body was supported by the rear legs and moved by assisting track driving in ③. Finally, the robot released its rear legs and completed the motion in ④.

In the experiment for the gap width of 300 mm, the detected gap width was $W = 318.9$ mm, and became $L_h < W$. Therefore, the robot determined that it was unable to perform gap traversing and stopped.

The error ratios of the detected gap widths were 2.6%, 6.6%, and 6.3% for gap widths of 100, 200, and 300 mm, respectively. Compared with the results in **Table 2**, the error ratio increased by approximately 1.1% at 300 mm. We assumed that the error was influenced by negligible changes in the robot's position and disturbances in the actual environment. However, it decreased in the 200 mm gap width. Therefore, we assumed that an accurate gap width detection was performed in this experiment.

From these results, we confirmed that the traversing motion was appropriately and safely selected by the robot according to the detected gap width.

6. Discussion

The proposed method was based on the assumptions described in Sections 3.1 and 4.2, and simulations and experiments were performed. However, these conditions may not be applicable to a real environment. The following sections discuss the applicability of the proposed method when each condition is infeasible.

6.1. Gap Width

If the width of the gap is not constant, the gap widths on the left and right tracks diverge. In this case, it is necessary to detect and calculate the gap widths on both the left and right lines of the tracks. Then, the gap width W required to determine the action becomes the distance between the nearer and farther edges. The traversing motion can be performed via the proposed method, behaving as if a parallel edge of the distance exists.

Accordingly, this challenge can be addressed by installing two of the distance measurement systems presented in this study to detect the widths of the left and right gaps.

When the robot is not orthogonal to the gap, the same limitation can be addressed, and thus the same solution can be adopted by the proposed method.

6.2. Height of Ground

If the heights of the ground between the gaps are different, it is necessary to consider a traversing motion for the gap with a step. For example, it will be effective for the robot to alter the posture of the body, such that it is the angle formed by the front and rear edges of the gap during the gap traversal. This motion was performed in the same manner as the proposed method.

Regarding the detection of the gap with a step, the road surface on the far side cannot be detected when it is higher than the distance measurement system. In this case, the edge on the far side may be detected from the initial sensing position on the wall. However, it may be difficult to perform gap traversal because the road surface is not detected. If the distance measurement system is mounted on the higher part of the robot to allow surface detection, the motion will be feasible via the proposed method. Even if it is possible, we need to carefully decide a sufficient height for the sensor because the down slope case should also be taken into account.

6.3. Shape of Gap Edge

If the gap edge is not sharp, such as a round or sloped edge, the amount of change in the measured distance presented in Section 4.2 may not be obtained sufficiently, and a significant error may occur in the position detection of the edge.

In the case of a small round or sloped edge, introducing a safety margin to the L_l and L_h values, as presented in Section 3.2, may be beneficial.

Otherwise, for a large round or sloped edge, the gap width can be calculated by the intersection of the extended road and wall surfaces as the virtual gap edge. The road and wall surfaces may be detected by a 2-D point cloud obtained from the distance measurement system.

6.4. Posture of Wall in Gap

Consider the case in which the wall surface in the gap is not vertical.

When the angle between the wall and road surfaces on the far side is negligible, such as a steep cliff, the distance on the wall surface will not be detected. In this case, because the maximum detection length of the sensor is provided as the distance information when it cannot be detected, the distance increases abruptly after the gap edge. Therefore, the proposed method can be applied without issues.

However, if the wall inclines steadily and the angle between the wall and road surfaces is significant and obtuse, the derivative of the measured distance will not change from negative to positive on the gap edge; thus, autonomous gap traversing via the proposed sensing method will become difficult. In this case, another method, such as shape detection via a 3-D point cloud, is required.

6.5. Shape of Road Surface

Finally, we consider the case in which the road surface shape is not flat.

If a significant unevenness exists on the surface, it may be difficult to apply the proposed method owing to the false edge detection because the distance on the road surface does not change linearly.

In such a case, it will be necessary to include a method for detecting road and wall surfaces in addition to the proposed sensing method. For example, it may be effective to employ a smoothing filter to discard abrupt changes in distance.

7. Conclusion

In this study, we proposed a gap width detection method using a 2-D distance measurement system and an autonomous gap traversal motion based on the detected gap width obtained with a hexapod tracked mobile robot. The effectiveness of the proposed measurement system was confirmed by the results obtained from gap width measurements. In addition, the autonomous motion according to the gap width detected by the robot was confirmed experimentally. In the future, we will consider autonomous traversal for a gap with a step.

References:

[1] K. Ueda, M. Guarnieri, T. Inoh, P. Debenest, R. Hodoshima, E. Fukushima, and S. Hirose, "Development of HELIOS IX: An Arm-Equipped Tracked Vehicle," J. Robot. Mechatron., Vol.23, No.6, pp. 1031-1040, 2011.

[2] T. Kamegawa, T. Yamasaki, and F. Matsuno, "Evaluation of Snake-like Rescue Robot "KOHGA" for Usability of Remote Control," Proc. of IEEE Int. Workshop on Safety, Security and Rescue Robotics (SSRR 2005), pp. 25-30, 2005.

[3] A. Sinha and P. Papadakis, "Mind the gap: Detection and traversability analysis of terrain gaps using LIDAR for safe robot navigation," Robotica, Vol.31, Issue 7, pp. 1085-1101, 2013.

[4] E. Mihankhah, A. Kalantari, E. Aboosaeedan, H. D. Taghirad, S. Ali, and A. Moosavian, "Autonomous staircase detection and stair climbing for a tracked mobile robot using fuzzy controller," 2008 IEEE Int. Conf. on Robotics and Biomimetics, pp. 1980-1985, 2009.

[5] T. Fujita, T. Sasaki, and Y. Tsuchiya, "Hybrid Motions by a Quadruped Tracked Mobile Robot," Proc. of 2015 IEEE Int. J. on Safety, Security, and Rescue Robotics (SSRR 2015), pp. 1-6, 2015.

[6] T. Fujita and T. Sasaki, "Consideration on a Crawler Robot with Six Legs," Proc. of the 2016 Int. Conf. on Artificial Life and Robotics (ICAROB 2016), pp. 88-91, 2016.

[7] T. Fujita and T. Sasaki, "Development of Hexapod Tracked Mobile Robot and Its Hybrid locomotion with Object-Carrying," 2017 IEEE Int. Symp. on Robotics and Intelligent Sensors (IRIS 2017), pp. 69-73, 2017.

[8] I. Hayasi, "Tank-Technology," Sankaido, 1992 (in Japanese).

[9] T. Kinugasa et al., "Shelled Structure for Flexible Mono-tread Mobile Track," Int. J. of Applied Electromagnetics and Mechanics, Vol.52, Nos.3-4, pp. 891-896, 2016.

[10] T. Kamegawa, T. Yarnasaki, H. Igarashi, and F. Matsuno, "Development of the snake-like rescue robot "kohga"," Proc. of 2004 IEEE Int. Conf. on Robotics and Automation (ICRA '04), Vol.5, pp. 5081-5086, 2004.

[11] R. Hodoshima, Y. Fukumura, H. Amano, and S. Hirose, "Development of track-changeable quadruped walking robot TITAN X-design of leg driving mechanism and basic experiment," 2010 IEEE/RSJ Int. Conf. on Intelligent Robots and Systems, pp. 3340-3345, 2010.

[12] E. Rohmer et al., "Quince: A collaborative mobile robotic platform for rescue robots research and development," 2010 JSME/RMD Int. Conf. on Advanced Mechatronics (ICAM 2010), Vol.2010.5, pp. 225-230, 2010.

[13] S. Suzuki, S. Hasegawa, and M. Okugawa, "Remote control system of disaster response robot with passive sub-crawlers considering falling down avoidance," ROBOMECH J., Vol.1, No.1, pp. 1-12, 2014.

[14] S. Murakami, T. Ono, and T. Kimura, "Development of open source oriented working components for small mobile robots – Case study in RoboCup2019 Japan Open Nagaoka Rescue Real Machine League –," Proc. of the 2020 JSME Conf. on Robotics and Mechatronics, 2P2-C07, 2020 (in Japanese).

[15] S. Kobayashi, Y. Kobayashi, Y. Yamamoto, T. Watasue, Y. Ohtsubo, T. Inoue, and T. Takamori, "Development of a door opening system on rescue robot for search "UMRS-2007"," 2008 SICE Annual Conf., pp. 2062-2065, 2008.

[16] A. Motila and K. Kurt, "Real-time localization in outdoor environments using stereo vision and inexpensive gps," 18th Int. Conf. on Pattern Recognition (ICPR'06), Vol.3, pp. 1063-1068, 2006.

[17] K. N. Al-Mutib, E. A. Mattar, M. M. Alsulaiman, and H. Ramdane, "Stereo vision SLAM based indoor autonomous mobile robot navigation," 2014 IEEE Int. Conf. on Robotics and Biomimetics (ROBIO 2014), pp. 1584-1589, 2014.

[18] B. Joydeep and V. Manuela, "Depth camera based indoor mobile robot localization and navigation," IEEE Int. Conf. on Robotics and Automation, pp. 1697-1702, 2012.

[19] P. Kim, J. Chen, and Y. K. Cho, "SLAM-driven robotic mapping and registration of 3D point clouds," Automation in Construction, Vol.89, pp. 38-48, 2018.

[20] M. Nomatsu, Y. Suganuma, Y. Yui, and Y. Uchimura, "Development of an Autonomous Mobile Robot with Self-Localization and Searching Target in a Real Environment," J. Robot. Mechatron., Vol.27, No.4, pp. 356-364, 2015.

[21] K. Kurashiki, M. Aguilar, and S. Soontornvanichkit, "Visual Navigation of a Wheeled Mobile Robot Using Front Image in Semi-Structured Environment," J. Robot. Mechatron., Vol.27, No.4, pp. 392-400, 2015.

[22] N. Andreas, L. Kai, H. Joachim, and S. Hartmut, "6D SLAM – 3D mapping outdoor environments," J. of Field Robotics, Vol.24, Nos.8-9, pp. 699-722, 2007.

[23] T. Luka, Š. Igor, and K. Gregor, "Using a LRF sensor in the Kalman-filtering-based localization of a mobile robot," ISA Trans., Vol.49, No.1, pp. 145-153, 2010.

[24] H. Yu, H. Hsieh, Y. Tasi, Z.-H. Ou, Y. Huang, and T. Fukuda, "Visual Localization for Mobile Robots Based on Composite Map," J. Robot. Mechatron., Vol.25, No.1, pp. 25-37, 2013.

[25] Z. Taha, J. Chew, and H. Yap, "Omnidirectional Vision for Mobile Robot Navigation," J. of Advanced Computational Intelligence and Intelligent Informatics, Vol.14, No.1, pp. 55-62, 2010.

Name:
Taiga Sasaki

Affiliation:
Department of Electrical and Electronic Engineering, Faculty of Engineering, Tohoku Institute of Technology

Address:
35-1 Yagiyama Kasumi-cho, Taihaku-ku, Sendai 982-8577, Japan

Brief Biographical History:
2016 Received Bachelor of Engineering from Tohoku Institute of Technology
2018 Received Master of Engineering from Tohoku Institute of Technology
2018- Doctor Student, Tohoku Institute of Technology

Main Works:
• T. Fujita and T. Sasaki, "Development of Hexapod Tracked Mobile Robot and Its Hybrid locomotion with Object-Carrying," 2017 IEEE Int. Symp. on Robotics and Intelligent Sensors (IRIS 2017), pp. 69-73, 2017.

Membership in Academic Societies:
• The Society of Instrument and Control Engineers (SICE)

Name:
Toyomi Fujita

Affiliation:
Department of Electrical and Electronic Engineering, Faculty of Engineering, Tohoku Institute of Technology

Address:
35-1 Yagiyama Kasumi-cho, Taihaku-ku, Sendai 982-8577, Japan

Brief Biographical History:
1997- Research Associate, The University of Electro-Communications
2001- Visiting Researcher, University of California
2007- Associate Professor, Tohoku Institute of Technology
2014- Professor, Tohoku Institute of Technology

Main Works:
• T. Fujita and C. M. Privitera, "Robot Hand Movement Detection based on Top-Down and Bottom-Up Scanpath Prediction," Procedia Engineering, Vol.41, pp. 1162-1168, 2012.

Membership in Academic Societies:
• The Institute of Electrical and Electronics Engineers (IEEE)
• The Robotics Society of Japan (RSJ)
• The Society of Instrument and Control Engineers (SICE)